



Mechanisms of destructing translational domains in passive margin salt basins: Insights from analogue modelling

Zhiyuan Ge^{1*}, Matthias Rosenau², Michael Warsitzka^{3,2} and Rob L. Gawthorpe¹

¹ Department of Earth Science, University of Bergen, Allégaten 41, 5007 Bergen, Norway

² Helmholtz Center Potsdam, German Research Center for Geosciences - GFZ Potsdam, Germany

³ Institute of Geophysics of the Czech Academy of Sciences, Boční II/1401, 141 31 Prague 4, Czech Republic

Correspondence to: Zhiyuan Ge (Zhiyuan.Ge@uib.no)

Abstract. Current gravitational tectonics models illustrating the structural style of passive margin salt basins typically have domains of upslope extension and corresponding downslope contraction, separated by a domain of rather undeformed mid-slope translation. However, such a translational domain is rarely observed in natural systems where extensional and contractional structures may interfere in the mid-slope area. In this study, we use sandbox analogue modelling analyzed by 4D digital image correlation (DIC) to investigate how the pre-kinematic layer thickness, differential sediment loading and sedimentation rate control the structural evolution of translational domains. As in nature, experimental deformation is driven by slowly increasing gravitational forces associated with continuous basal tilting. The results show that a translational domain persists throughout the basin evolution when the pre-kinematic layer is evenly distributed, although a thin (1 mm in the experiment, 100 m in nature) pre-kinematic layer can render the translational domain relatively narrow when comparing to settings with a thicker (5 mm) pre-kinematic layer. In contrast, early differential sedimentary loading in the mid-slope area creates minibasins intervened by salt diapirs overprinting the translational domain. Similarly, very low sedimentation rate (1 mm per day in the experiment, equates to < 17 m/Ma in nature) in the early stage of the experiment results in an immature translational domain quickly overprinted by downslope migration of the extensional domain and upslope migration of the contractional domain. Our study suggests that the architecture of passive margin salt basins is closely linked to the sedimentary cover thickness and sedimentation pattern and rate. The translational domain, as an unformed region in the supra-salt cover, is likely a transient feature in nature and destructed in passive margins with either low sedimentation rate or a heterogeneous sedimentation pattern.

Keywords translational domain, thin-skinned, salt tectonics, passive margin, analogue modelling, digital image correlation (DIC)



1. Introduction


In passive margin basins containing syn- and post-rift salt deposits, salt tectonics generally have significant influences on structural style and stratigraphic architecture (Rowan, 2014). As the margin tilts due to thermal subsidence or seaward progradation of sedimentary wedges, passive margin salt basins often experience deformations related to gravitational failure (Brun and Fort, 2011; Rowan et al., 2004). Such gravitational failure is generally characterized by a kinematically linked system of upslope extension and downslope contraction enclosing a more or less undeformed translational domain, using the salt beneath as a detachment layer (Fig. 1a) (Brun and Fort, 2011; Cramez and Jackson, 2000; Dooley et al., 2017; Fort et al., 2004; Rowan et al., 2004).

While the translational domain has received little attention so far, the extensional and contractional domains have been studied extensively. For example, numerous studies have focused on structural style and kinematic evolution of rotated fault blocks (Mauduit et al., 1997), rollovers (Krézsek et al., 2007; Mauduit and Brun, 1998) and extensional diapirs (Koyi, 1998; Vendeville and Jackson, 1992a, b) in the extensional domain, and folds and thrusts (Duffy et al., 2018; Fort et al., 2004; Rowan et al., 2004), salt nappes and canopies (Hudec and Jackson, 2009; Hudec and Jackson, 2004; Masrouhi et al., 2013; Rowan et al., 2004) in the contractional domain. Conceptual models of salt-bearing passive margins commonly reduce the translation domain to a rather passive region of the cover strata, which widely remains undeformed during basin wide gravitational gliding and spreading (Fig. 1a) (e.g. Adam et al., 2012a; Fort et al., 2004). However, sub-surface data lacks evidence of such a clear undeformed translational domain in most passive margin salt basins, such as those in the West Africa and Brazilian margins (Fig. 1b and c). To our best knowledge, only one study so far has interpreted a typical translational domain based on 2D regional seismic analysis (Gradmann et al., 2005). However, such interpretation has been challenged by more recent, high quality 2D and 3D seismic analysis, suggesting widespread faulting in the translational domain (Gvirtzman et al., 2015). Instead, most passive margin salt basins have typical structures of minibasins and salt diapirs in the mid-slope area (Fig. 1b and c).


The concept of a translational domain is rather loosely defined because it has both structural and kinematic meanings. When used as a term describing the basin-wide structural partitioning, the translational domain usually indicates an area located between the upslope extensional and downslope contractional structures (e.g. Fig. 1a). For example, when describing the structural character of the Lower Congo Basin, Rowan (2014) used the term of translational domain to indicate the mid-slope area of salt minibasins and diapirs. Yet many diapirs and minibasins in the mid-slope have an extensional or contractional origin, due to the down- and up-slope migration of



extensional and contractional domains, respectively (Brun and Fort, 2011; Fort et al., 2004). When one refers to the kinematic behaviour of the salt basin, the translational domain means a zone within the salt basin that is transferring the deformation without internal deformation (e.g. Adam et al., 2012a). In this sense, the translational domain may not be part of the final basin architecture, but only present during the basin evolution. To avoid any confusion, we refer the translational domain here satisfying two criteria, i.e. being a largely undeforming (at least transiently) area and connects upslope extension and downslope contraction.

In this study, we aim to investigate the structural evolution of the passive margin's mid-slope area and the origin of a translation domain in a salt basin setting. Using analogue sandbox modelling combined with quantitative surface deformation monitoring by means of 4D (3D plus time  (digital image correlation), we demonstrate how the translation domain **originates and evolves and ascertain** possible mechanisms on how it can be destroyed during ongoing gravity gliding. Specifically, we focus on the influences of pre-kinematic layer thickness, differential sedimentary loading and sedimentation rate on the structural evolution of the translation domain. Furthermore, we investigated the overall evolution of different kinematic domains to understand the complexity of kinematic domains and how they develop through time and space.


2. Analogue modelling methods

Analogue experiments of gravitationally driven salt tectonic processes using granular rock analogue materials, such as sand to model the supra-salt cover sediment and  silicone oil to model **salt layers**, have been traditionally explored to get insight into thin-skinned salt tectonics (Ge et al., 1997; Mauduit and Brun, 1998; Mauduit et al., 1997; Rowan and Vendeville, 2006; Vendeville and Jackson, 1992b), as well as basin-scale geometry and evolution (Adam and Krezsek, 2012; Fort et al., 2004). In the last decade, the advent of quantitative and high resolution 4D DIC (digital image correlation) techniques, which records time series of incremental experimental surface deformation in 2D and 3D, allows the analysis and reconstruction of the kinematic evolution of basin-wide structures in high detail and accuracy (Adam et al., 2012a; Adam and Krezsek, 2012).

2.1 Rock analogue materials



In this study, we use granular materials to simulate the brittle sediment layer cover and PDMS (polydimethylsiloxane) silicone oil to represent the viscous salt underneath. The density contrast between commonly used pure quartz sand and silicone in analogue modelling is generally too high when comparing to natural prototypes (Allen and Beaumont, 2012). In unison with other studies




(Adam et al., 2012a; Dooley et al., 2007), we hereby use a mixture of quartz sand (G12, grain size: $<400 \mu\text{m}$) and foam glass spheres (company: LIAVER, grain size: $250\text{--}500 \mu\text{m}$) to adjust the density ratio between the cover layer and silicone. The weight ratio for a mixture of sand and foam glass sphere is 3:1 and the resulted mixture density is 1.13 g/cm^3 after si g. The resulting
 5 density ratio between the granular mixture and silicone is 1.16, which is representative for a
 density ratio between cover sediments and underlying salt (Adam et al., 2012a; Allen and
 Beaumont, 2012; Warsitzka et al., 2015).

The frictional properties of the granular mix are similar to pure sands used in analogue modelling
 (e.g. Klinkmüller et al., 2016). Static and sliding friction coefficients of the granular mixture are
 10 about 0.7 and 0.55 respectively, and cohesion is in the order of few tens of Pa as determined using
 a ring shear tester (Schulze RST-01.pc, Schulze reference, for more details see Warsitzka et al.
 (2018)). The silicone used in the experiments (Bayer Korasilon G30M) has a density of 0.97 g/cm^3
 at temperature of 25°C with a Newtonian viscosity of about $2 \times 10^4 \text{ Pa s}$ at shear rates below 10^{-1} s^{-1}
¹ (Rudolf et al., 2016) as realized in the experiments reported here.

15 2.2 Model scaling

Adequate scaling of the analogue model from the natural prototype allows a direct comparison
 between the model and the natural prototype in terms of geometry, kinematic evolution as well as
 the deformation driving and resisting forces (Costa and Vendeville, 2002; Hubbert, 1937; Ramberg,
 1981). Based on dimensionless numbers representing ratios of forces, scaling factors for the basic
 20 dimensions of length, mass and time are derived. Here we use the ratio of lithostatic pressure vs.
 cohesion and the Ramberg umber relating gravitation and viscous strength to derive scaling
 factors (e.g. Adam and Krezsek, 2012; Gemmer et al., 2005). Among all the scaling factors, the
 geometric (l^*) and time (t^*_{sm})  scaling factors are particularly important to understand the model
 design and interpretation. In this study, the geometric scaling, as constrained by cohesion and
 25 densities of the rock analogue versus rocks is $l^* = 10^{-5}$ (1 cm in model is 1 km in nature). The
 time scaling, dictated by the viscosity of salt versus PDMS, is then $t^*_{\text{sm}} = 4.255 \times 10^{-10}$ (4 hours
 in the model is approximately 1 Ma in nature). See Appendix Table A1 for scaling relations.

2.3 Experimental setup and model design

As this study aims to understand kinematic domain partition and evolution in passive margin salt
 30 basin, the overall setup of the apparatus shares the characteristics of earlier studies (Fig. 2) (Adam
 et al., 2012a; Fort et al., 2004) . A flat rigid base of 1 m wide and 1.8 m long is covered by a basal
 sand layer with a double-wedge shape akin to passive margin basins (Brun and Fort, 2011, 2012).



The two wedges are 65 cm and 25 cm in length and 90 cm wide (Fig. 2a). The asymmetric basin formed by the wedges is subdivided by a 4 cm wide sand ridge along its symmetry axis separating two 35 cm wide and 90 cm long asymmetric basins filled with silicone (Basin a and Basin b) (Fig. 2a). The silicone thickness is 2 cm at the basin's deepest location and pinches out towards the basins margins (Fig. 2a). The tilting of the entire base towards the steeper basin side downslope is driven by a computer-controlled stepper motor at a continuous rate of 1° per day.

Each of the experiments takes about ten days from preparation to slicing. The silicone is filled in the silicone basin at least 3 days to settle. Once the silicone is free from air bubbles and has a flat surface, a pre-kinematic layer of the quartz sand – foam glass beads mixture is sieved onto the silicone surface. Then, tilting is started at the rate of 1° per day until reaching a final tilting position of 3.5° after 64 hours. Subsequently, the experiment continues for another 36 hours under static conditions. The total running time is consequently 5 days or 120 hours, which equals to approximate 30 Ma in the natural prototype (Appendix Table A2). During the experiment, the granular material is added by sieving within about twenty minutes onto the model surface every 12 hours to simulate syn-kinematic sedimentation (Appendix Table A2). After the experiment, the model surface is covered with sand before being gelled, sliced and photographed.

Overall three experiments were carried out for the purpose of this study and sedimentation patterns were varied for the two sub-silicone basins throughout the three experiments:

1. Experiment 1 (basins 1a and 1b) aims to investigate the impact of pre-kinematic layer thickness on the development of the translational domain. In Basin 1a, the pre-kinematic layer was 1 mm thick and further sedimentation was added every 12 hours with an overall wedge shape and 1 mm average thickness (Fig. 3). Basin 1b had the same syn-kinematic sedimentation rate as the Basin 1a, but with a pre-kinematic layer of 5 mm (Fig. 3).
2. Experiment 2 (basins 2a and 2b) tests how differential loading and minimum sedimentation influence the translational domain. The syn-kinematic sedimentation was the same as in experiment 1 (Fig. 3). However, the pre-kinematic layer in Basin 2a was 1 mm thick in average, but with a differential sedimentation pattern of 8 minibasins created by sieving. The minibasins were 3–4 cm wide with 6–7 cm gaps in between. Minibasin spacing and dimensions are constrained by generalization of natural observations (Carreras and Jackson, 2000; Hudec and Jackson, 2004; Marton et al., 2000). The differential sieving continued for 36 hours before sieving of sedimentary wedges started again (Fig. 3). Basin 2b, in contrast, had an even thickness of 1 mm for the pre-kinematic layer (Fig. 3). Further



sedimentation was only added to cover the exposed, reflective silicone to allow the monitoring system to work properly (Appendix Table A2). Thus, sieving rate on average in this silicone basin was very low.

3. Experiment 3 investigates the translational domain development under a thin pre-kinematic layer and low sedimentation rate. Both Basin 3a and 3b had pre-kinematic layers of 0.5 mm thickness and sedimentation rates of 0.5 mm per 12 hours (Fig. 3). However, differential loading was created in Basin 3a by three minibasins in the upslope area with similar geometry to those in Basin 2a (Fig. 3). The syn-kinematic differential sedimentation also continued for three sieving periods before wedge shaped syn-kinematic sedimentation was applied (Appendix Table A2).

2.4 Experimental monitoring

We apply state-of-the art strain monitoring methods based on digital image correlation (DIC) to derive quantitative observational data from the experiments. The evolving model surface is monitored by a stereoscopic pair of two digital 12-bit monochrome CCD cameras with 29 mega pixels (LaVision Imager X-Lite 29M) at a time interval of 100 s (0.01 Hz frequency). We attach the cameras and an LED system to a frame moving with the base. Thereby only deformation with respect to the base is recorded, i.e. gravity gliding without interfering with the tilting motion. The recorded stereoscopic images are processed with digital image correlation (DIC) techniques which allows deriving the surface topography and full 3 dimensional incremental surface velocity field with high accuracy (≤ 0.1 px) (Adam et al., 2005). We use Davis Strainmaster 8 by LaVision software applying least square methods (LSM) algorithms.

The DIC analysis yields quantitative deformation information of the experiment surfaces, such as incremental and cumulative horizontal (V_x) and vertical displacements (V_z), i.e. subsidence and uplift. From the surface velocities the incremental longitudinal strain (ϵ_{xx}) along the symmetry axis of the models (downslope) are derived (strain profile data). DIC analysis allows us to quantitatively constrain and analyze the structural and kinematic evolution of the model at high spatial (resulting vector spacing about 1-2 mm, at a vector accuracy of few tens of microns) and sufficient temporal resolution (100 seconds). Digital image correlation data generated in this study is published open access in Ge et al. (2019).

3. Experimental observations and modelling results



To describe the model structural evolution both qualitatively and quantitatively, we visualize DIC-derived data as maps of surface incremental displacement and strain, as well as space-time plots of strain profile data (i.e. strain evolution plots) in combination with cross sections of the finite models to demonstrate the temporal and spatial evolution of kinematic domains and individual structures. Representative surface displacements and longitudinal strains from three intervals—25–36 hours, 61–72 hours and 109–120 hours—represent the surface geometry and evolution from early, mid and later stages of the experiments (e.g. Fig. 4). The strain evolution plots visualize the surface strain evolution in the centre of each silicone basin through time (e.g. Fig. 5a). The strain evolution plots are tied to the cross sections showing the exact location of the structures and their spatial and temporal evolution as seen at the model surface (e.g. Fig. 5a).

3.1 Experiment 1

In experiment 1, after the first period of syn-kinematic sieving both silicone basins 1a and 1b are dominated by gravity gliding with upslope extension and downslope contraction (Fig. 4). However, in the early stage of Basin 1a, where the pre-kinematic layer is 1 mm thick, an *c.* 10 cm wide belt with extensional grabens and diapirs occurs at the uppermost edge of the slope. Downdip, two significant thrusts and folds develop with an interval of *c.* 10 cm near the lowermost edge of the silicone basin (ϵ_{xx} in Fig. 4a). In contrast, in Basin 1b, the cover layer remains largely undeformed in the early stage as only a single extensional graben develops at the upslope tip and no visually resolvable contractional structures occur in the downslope (ϵ_{xx} in Fig. 4a).

In Basin 1b, major deformation starts in the mid stage when a thrust belt T_{b1} occurs *c.* 10 cm away from the silicone basin tip in the downslope (ϵ_{xx} in Fig. 5b). In the late stage, a frontal thrust T_{b2} occurs at the tip of the silicone basin (ϵ_{xx} in Fig. 5b). However, as the front thrust T_{b2} is initiated, the early thrust T_{b1} gradually becomes inactive (Fig. 5b). At the same time in Basin 1a, the thrust belt shifts towards the basin tip of the downslope as well as the upslope and both thrust belts keep active into the late stage (ϵ_{xx} in Fig. 5a). Consequently, the contractional domain in Basin 1a is larger than that in Basin 1b at the end of the experiment (Fig. 5a and b). As both extensional domains of basins 1a and 1b are 20 cm long along dip direction, the resultant translational domain is smaller in Basin 1a (*c.* 40 cm) compared to that (50 cm) of Basin 1b (Fig. 5a and b). In short, both basins 1a and 1b show a clear domain partitioning from extension through translation to contraction, as described in the classic conceptual model (Fig. 1a).

3.2 Experiment 2

In experiment 2, two silicone basins 2a and 2b show considerable differences in structural style



and evolution due to different sedimentation patterns. In Basin 2a, differential loading of the pre-kinematic layer and early syn-kinematic sieving results in a basin-wide imprint of minibasins downbuilding, as shown by the subsidence pattern during the early stage where strings of thicker pre-kinematic layer subside stronger than intervened regions forming minibasins (Vz in Fig. 6a).

How minibasin downbuilding only dominates the deformation for a very short period of about 1 to 2 hours during which the minibasins extend and areas in between are affected by diapirism and contraction (Fig. 7a). Shortly afterwards, gravity gliding takes over as extension dominated upslope and contraction dominated the downslope (Fig. 7a). During the transition, the minibasin area (apart from Minibasin 1) becomes a shadow zone of deformation and transfer strain passively while the diapirs start to accommodate deformation (Fig. 7c).

In the mid and late stages, Basin 2a develops similar surface pattern to the basins in the experiment 1 with clear domains of extension, translation and contraction (Fig. 7a). In contrast, Basin 2b has a different structural style and basin evolution comparing to Basin 2a. Since Basin 2b has the same pre-kinematic layer thickness as in Basin 1b, the evolution of kinematic domain partitioning from early to mid stage are similar in both experiments. However, in Basin 2b, as there is no syn-kinematic sedimentation in the early stage and only minimum sedimentation afterwards (Appendix Table A2), extensional structures are initiated in a wider area of c. 30 cm along dip and grow even larger to more than 40 cm in late stage (Figs 6a and 7b). Contractional structures occur in an area of c. 20 cm along dip near the tip of the downslope of the Basin 2b (Fig. 7b). The contractional belt converges into a area of approximately 10 cm wide before the contraction migrates upslope in the later stage (Figs 6c and 7b). Due to the thin cover layer in the mid-slope (~ 1 mm), the migration of the contractional domain upslope causes short-wavelength folding in the translational domain (Fig. 7b). At the end of the experiment, the contractional domain overlaps with previous extensional domain, causing squeezing of extensional diapirs and deformation of the cover layer in the former translational domain (Fig. 7b).

3.3 Experiment 3

In experiment 3, both silicone basins 3a and 3b have a pre-kinematic layer of 0.5 mm and a syn-kinematic sedimentation rate of 0.5 mm/12 hours. As a result, the structural evolution of both basins share many similarities (Fig. 8). The only difference is that three minibasins are created in the upslope of the pre-kinematic layer in Basin 3a while the pre-kinematic layer has even thickness in Basin 3b. Sieving of these minibasins continues three periods (Appendix Table A2).

In Basin 3a, differential loading dominates the upslope deformation briefly in the first 1–2 hours



of the experiment (Fig. 10a), similar to what is observed in Basin 2a (Fig. 7c). However, since the minibasins are located only in the upslope area of Basin 3a and the sieving rate is half compared to Basin 2a, the imprint of minibasin downbuilding on the structural evolution is less significant comparing to Basin 2a. For example, the diapir preserved between the minibasins 2 and 3 in the cross section has limited height and is much smaller than similar diapirs in Basin 2a (Fig. 9a).

Importantly, the differential loading in Basin 3a also influences the development of extensional structures. For example, the extensional grabens develop earlier in Basin 3a than those in Basin 3b (Fig. 9a and b). Similarly, the upslope migration of the contractional domain also starts early in Basin 3a, as many small wavelength folds occur in the former translational domain at 60 hours and afterward (Figs 8b and 9a). In contrast, the upslope migration of contraction occurs after 84 hours in Basin 3b (Figs 8c and 9b). By the end of the experiment, in both basins 3a and 3b, upslope migrated contractional structures interfere with early extensional structures, resulting in a deformed translational domain (Fig. 9a and b).

4. Discussion

We used basin-scale sandbox analogue modelling to study the first order controls on origination, development and destruction of the translational domain in salt-bearing passive margin basins where the thin-skinned salt tectonics dominates the structural and stratigraphic evolution. Based on the analysis of temporal and spatial evolution of kinematic domains and individual structures, we identify the translational domain as a transient feature destructed by two potential mechanisms: i) migration of extensional and contractional domains into a previous undeformed translational domain; ii) differential loading by sedimentation into minibasins that triggers salt-related structures, such as diapirs, from the beginning of basin evolution therefore prevents the formation of a tectonically stable translational domain.

4.1 Control of pre-kinematic layer thickness and sedimentation rate on formation of a translational domain

Our modelling results are in good agreement with previous works where a translational domain is evident when a relatively thick and continuous homogeneous pre-kinematic layer exists. Translational domains have been observed with a pre-kinematic layer of even thickness in the order of 3–10 mm (300 to 1000 meters in nature) (Adam et al., 2012a; Adam and Krezsek, 2012; Fort et al., 2004). Similar observations are derived from this study where about 50% of the basin length is occupied by the translational domains within basins 1a and 1b (Fig. 5). As noted by Brun



and Fort (2012), the cover layer needs to be thick and strong enough to transfer the strain without deforming internally. In many analogue models, the total thickness of pre- and syn-kinematic layers is usually on the order of a few centimetres (e.g. Adam et al., 2012a; Fort et al., 2004), which equals to a few kilometres in nature using a similar geometric scaling factor from this study (1 cm in model is 1 km in nature). According to our study, a 1 mm thick pre-kinematic layer and 2-3 mm sediment from syn-kinematic sedimentation (few hundreds of meters if scaled to nature) seems strong enough to form a stable translational domain from beginning to end, such as in Basin 1a (Fig. 5a).

4.2 Translational domain destruction by deformation migration

Our study shows that a very thin supra-salt cover, combining a thin pre-kinematic layer with a very low sedimentation rate, allows the downslope migration of extensional domains and upslope migration of contractional domains, which ultimately leads to the destruction of the translational domain (Fig. 10a). Specifically, when the pre-kinematic layer is only 0.5 mm in the models (50 m in nature) and sedimentation is 1 mm/day (about 17 m per Ma in nature), the translational domain can be destroyed by the migration of extension and contraction towards the basin centre (Fig. 10a and b). However, the simulated sedimentation rate of about 17 m/Ma in nature is extremely low comparing to salt basins where the typical sedimentation rate is in the order of 100 m/Ma (Adam et al., 2012a; Adam and Krezsek, 2012). In general, such low sedimentation rates are more compatible with typical hemiplegic sedimentation rates of 2–20 m/Ma (Stow et al., 2001). This implies that our models including a very thin pre-kinematic layer and a very low sedimentation rate may be not archetypical passive margin salt basins where the terrigenous input is generally significant (Fig. 1b and c). Therefore, the first proposed mechanism for translational domain destruction by deformation migration might be active only in special geological settings where sediment supply is limited.

4.3 Translational domain destruction by differential loading

A more plausible mechanism for translational domain destruction suggested by our experiments is differential loading in the mid-slope along with the occurrence of minibasins and diapirs (Fig. 10b). In experiment 2, the basin-wide differential loading was applied in Basin 2a (Fig. 7a), which resulted in the formation of minibasins and diapirs. Even though the differential loading only dominated the basin for a short early period (roughly 1.5 hours in the model or 0.375 Ma in nature), the translational domain was completely deformed. Although the pattern of differential loading is idealized in the experiments, similar sedimentation patterns might persist in nature as



natural sedimentary systems deliver variable sediment supply through alternating fairways resulting in different sediment thicknesses across the basin.

For example, restorations of the earliest stratigraphic units in passive margin salt basins have always been patchy with various thicknesses in different locations (Adam et al., 2012b; Hudec and Jackson, 2004; Marton et al., 2000). Moreover, numerical simulation has demonstrated that such patchy pattern of minibasins intervened by salt diapirs can be simply formed by differential loading alone (Peel, 2014).

Since the scenario of early differential loading is more realistic than a thick and uniform supra-salt cover, the strain transfer from upslope extension to downslope contraction may not be through a

simple translational domain as current models suggest (Fig. 10a, 10b and d). The thick and strong minibasins and intervened weak diapirs form heterogeneity within sediment cover and complicate the pattern of strain transfer. For example, the minibasins in the Basin 2a were translated individually and the diapirs between accommodated the deformation in the early stage (Figs 7c and 10d). In this way, the deformation partially transfers from the upslope extension to the downslope contraction but is partially accommodated by minibasin translation and diapir squeezing in the mid-slope (Fig. 10d). A translational domain therefore is not necessary to be present during the whole evolution of the passive margin salt basins.

4.4 Alternative mechanisms for translation domain destruction

Other mechanisms may also be responsible for the destruction or nonexistence of a well-defined translational domain. One potential mechanism is sub-salt step or relief associated with early tectonic activity in passive margin salt basins (Jackson and Hudec, 2005; Pichel et al., 2018). Analogue models with sub-salt steps/relief have demonstrated that these basement structures can cause strain localization within the supra-salt cover strata therefore complicating the structural style and deforming the translational domain (Dooley et al., 2017; Dooley et al., 2018; Gaullier et al., 1993).

Moreover, progradational sedimentary wedges can also prevent the translational domain from forming. As the sedimentary wedges progressively move basinwards, early formed contractional structures are superimposed by late extensional structures, completely destroying the translational domain (Brun and Fort, 2011; McClay et al., 1998; Yonville, 2005). Although the sedimentary wedge is also one type of differential loading, the absence of tilting makes the system very different from the ones presented in this study. Future research therefore is needed to fully understand the influences of sub-salt structures and progradational wedges on the development and destruction of translational domains.



5. Conclusions

Sandbox analogue modelling analyzed by 4D digital image correlation (DIC) allowed a thorough and precise analysis of kinematic domain partitioning, as well as structural evolution of a passive margin salt basin under different pre- and syn-kinematic sedimentation patterns.

- 5 Experiments with uniform pre-kinematic cover thickness show a typical domain partition of upslope extension compensated by downslope contraction with an intermediate translational domain.

Under such circumstances, even very thin (1 mm) pre-kinematic cover was sufficient to generate the translational domain. For a thick cover, the translational domain persisted until the end of the
10 experiment.

We identified two scenarios in which the translational domain can be considered a transient feature destructed during the course of an experiment. First, when the initial cover layer is thin and sedimentation rate is low, upslope migration of the contractional domain completely overprints the translational domain. Second, when differential sediment loading is applied, formation of
15 minibasins intervened by diapirs in the mid-slope destructs the translational domain.

A comparison between models and natural cases suggests that an undeformed translational domain seen in analogue models rarely occurs in nature. This seems to be related to the general implementation of a thick, mechanically stable (or rigid undeformable) cover layer in analogue models neglecting the subtle initial thickness variations likely present in natural sedimentary
20 systems. Low sedimentation rate required for the destruction of the translational domain through migration of extensional and contractional domains as suggested by our study is also rare in natural passive margins. Instead, initial thickness variations within the cover creating differential loading and furthermore causing translational domain destruction through the formation of mid-slope minibasins and diapirs seems to be a more viable mechanism in nature.

- 25 **Data availability.** The experimental data, along with analysis code, are available on the GFZ repository (Ge et al., 2019).

Author contributions. ZG, MR and RG designed the experiments. ZG, MR and MW ran the experiments. ZG, MR and MW processed the data and did the strain analysis. All authors contributed to the writing of the manuscript.

- 30 **Competing interests.** The authors declare no conflict of interest.



Acknowledgement

The project was supported by E.ON Stipendienfonds and 2018 TNA program of EPOS' Thematic Core Service Multi-scale Laboratories. ZG would like to thank Equinor for sponsorship. We thank Frank Neumann and Thomas Ziegenhagen for construction of the experimental device as well as the whole laboratory team for scientific assistance. Danielle Howlett is thanked for remarks on an early version of the paper. We thank GFZ Data Services for making the data underlying this study open accessible (Ge et al., 2019; Warsitzka et al., 2018).

References

- Adam, J., Ge, Z., and Sanchez, M.: Post-rift salt tectonic evolution and key control factors of the Jequitinhonha deepwater fold belt, central Brazil passive margin: Insights from scaled physical experiments, *Marine and Petroleum Geology*, 37, 70–100, 2012a.
- Adam, J., Ge, Z., and Sanchez, M.: Salt-structural styles and kinematic evolution of the Jequitinhonha deepwater fold belt, central Brazil passive margin, *Marine and Petroleum Geology*, 37, 101–120, 2012b.
- Adam, J. and Krezsek, C.: Basin-scale salt tectonic processes of the Laurentian Basin, Eastern Canada: insights from integrated regional 2D seismic interpretation and 4D physical experiments, *Geological Society, London, Special Publications*, 363, 331–360, 2012.
- Adam, J., Urai, J. L., Wieneke, B., Oncken, O., Pfeiffer, K., Kukowski, N., Lohrmann, J., Hoth, S., van der Zee, W., and Schmatz, J.: Shear localisation and strain distribution during tectonic faulting—new insights from granular-flow experiments and high-resolution optical image correlation techniques, *J. Struct. Geol.*, 27, 283–301, 2005.
- Allen, J. and Beaumont, C.: Impact of inconsistent density scaling on physical analogue models of continental margin scale salt tectonics, *Journal of Geophysical Research: Solid Earth*, 117, 2012.
- Brun, J.-P. and Fort, X.: Salt tectonics at passive margins: Geology versus models, *Marine and Petroleum Geology*, 28, 1123–1145, 2011.
- Brun, J.-P. and Fort, X.: Salt tectonics at passive margins: geology versus models—Reply, *Marine and Petroleum Geology*, 37, 195–208, 2012.
- Costa, E. and Vendeville, B.: Experimental insights on the geometry and kinematics of fold-and-thrust belts above weak, viscous evaporitic décollement, *J. Struct. Geol.*, 24, 1729–1739, 2002.
- Cramez, C. and Jackson, M. P. A.: Superposed deformation straddling the continental-oceanic transition in deep-water Angola, *Marine and Petroleum Geology*, 17, 1095–1109, 2000.
- Dooley, T. P., Hudec, M. R., Carruthers, D., Jackson, M. P. A., and Luo, G.: The effects of base-salt relief on salt flow and suprasalt deformation patterns — Part 1: Flow across simple steps in the base of salt, *Interpretation*, 5, SD1–SD23, 2017.
- Dooley, T. P., Hudec, M. R., Pichel, L. M., and Jackson, M. P. A.: The impact of base-salt relief on salt flow and suprasalt deformation patterns at the autochthonous, paraautochthonous and allochthonous level: insights from physical models, *Geological Society, London, Special Publications*, 476, 2018.
- Dooley, T. P., Jackson, M. P. A., and Hudec, M. R.: Initiation and growth of salt-based thrust belts on passive margins: results from physical models, *Basin Research*, 19, 165–177, 2007.
- Duffy, O. B., Dooley, T. P., Hudec, M. R., Jackson, M. P. A., Fernandez, N., Jackson, C. A. L., and Soto, J. I.: Structural evolution of salt-influenced fold-and-thrust belts: A synthesis and new insights from basins containing isolated salt diapirs, *Journal of Structural Geology*, 114, 206–221, 2018.
- Fort, X., Brun, J.-P., and Chauvel, F.: Salt tectonics on the Angolan margin, synsedimentary deformation processes, *AAPG bulletin*, 88, 1523–1544, 2004.
- Gaullier, V., Brun, J. P., Guerin, G., and Lecanu, H.: Raft tectonics: the effects of residual topography below a salt de'collement, *Tectonophysics*, 228, 363–381, 1993.
- Ge, H., Jackson, M. P. A., and Vendeville, B. C.: Kinematics and dynamics of salt tectonics driven by progradation, *AAPG bulletin*, 81, 398–423, 1997.



- Ge, Z., Rosenau, M., Warsitzka, M., Rudolf, M., and Gawthorpe, R. L.: Digital image correlation data from analogue modeling experiments addressing mechanisms of destructing translational domains in passive margin salt basins. GFZ Data Services, <http://doi.org/10.5880/GFZ.4.1.2019.001>, 2019.
- 5 Gemmer, L., Beaumont, C., and Ings, S. J.: Dynamic modelling of passive margin salt tectonics: effects of water loading, sediment properties and sedimentation patterns, *Basin Research*, 17, 383–402, 2005.
- Gradmann, S., Hübscher, C., Ben-Avraham, Z., Gajewski, D., and Netzeband, G.: Salt tectonics off northern Israel, *Marine and Petroleum Geology*, 22, 597–611, 2005.
- Gvirtzman, Z., Reshef, M., Buch-Leviatan, O., Groves-Gidney, G., Karcz, Z., Makovsky, Y., and Ben-Avraham, Z.: Bathymetry of the Levant basin: interaction of salt-tectonics and surficial mass movements, *Marine Geology*, 360, 25–39, 2015.
- 10 Hoshino, K., Koide, H., Inami, K., Iwamura, S., and Mitsui, S.: Mechanical Properties of Tertiary Sedimentary Rocks under High Confining Pressure, Geological Survey of Japan, Kawasaki, Report, 244, 1972.
- Hubbert, M. K.: Theory of scale models as applied to the study of geologic structures, *Bulletin of the Geological Society of America*, 48, 1459–1520, 1937.
- 15 Hudec, M. R. and Jackson, M. P.: Interaction between spreading salt canopies and their peripheral thrust systems, *J. Struct. Geol.*, 31, 1114–1129, 2009.
- Hudec, M. R. and Jackson, M. P. A.: Regional restoration across the Kwanza Basin, Angola: Salt tectonics triggered by repeated uplift of a metastable passive margin, *AAPG Bull.*, 88, 971–990, 2004.
- 20 Jackson, M. P. A. and Hudec, M. R.: Stratigraphic record of translation down ramps in a passive-margin salt detachment, *Journal of Structural Geology*, 27, 889–911, 2005.
- Jaeger, J. C. and Cook, N. G. W.: Fundamentals of rock mechanics. Methuen & Co Ltd., London, 1969.
- Koyi, H.: The shaping of salt diapirs, *Journal of Structural Geology*, 20, 321–338, 1998.
- Krężsek, C., Adam, J., and Grujic, D.: Mechanics of fault and expulsion rollover systems developed on passive margins detached on salt: insights from analogue modelling and optical strain monitoring, *Geological Society, London, Special Publications*, 292, 103–121, 2007.
- 25 Lallemand, S. E., Schnürle, P., and Malavieille, J.: Coulomb theory applied to accretionary and nonaccretionary wedges: Possible causes for tectonic erosion and/or frontal accretion, *Journal of Geophysical Research: Solid Earth*, 99, 12033–12055, 1994.
- 30 Marton, G., Tari, G. C., and Lehmann, C. T.: Evolution of the Angolan Passive Margin, West Africa, With Emphasis on Post - Salt Structural Styles, Atlantic rifts and continental margins, 2000. 129 – 149, 2000.
- Masrouhi, A., Bellier, O., Koyi, H., Vila, J.-M., and Ghanmi, M.: The evolution of the Lansarine–Baouala salt canopy in the North African Cretaceous passive margin in Tunisia, *Geological Magazine*, 150, 835–861, 2013.
- 35 Mauduit, T. and Brun, J. P.: Growth fault/rollover systems: birth, growth, and decay, *Journal of Geophysical Research: Solid Earth*, 103, 18119–18136, 1998.
- Mauduit, T., Guerin, G., Brun, J.-P., and Lecanu, H. J. J. o. S. G.: Raft tectonics: the effects of basal slope angle and sedimentation rate on progressive extension, 19, 1219–1230, 1997.
- 40 McClay, K. R., Dooley, T., and Lewis, G.: Analog modeling of progradational delta systems, *Geology*, 26, 771–774, 1998.
- Modica, C. J. and Brush, E. R.: Postrift sequence stratigraphy, paleogeography, and fill history of the deep-water Santos Basin, offshore southeast Brazil, *AAPG bulletin*, 88, 923–945, 2004.
- Peel, F. J.: How do salt withdrawal minibasins form? Insights from forward modelling, and implications for hydrocarbon migration, *Tectonophysics*, 630, 222–235, 2014.
- 45 Pichel, L. M., Peel, F., Jackson, C. A. L., and Huuse, M.: Geometry and kinematics of salt-detached ramp syncline basins, *Journal of Structural Geology*, 115, 208–230, 2018.
- Ramberg, H.: Gravity, deformation, and the earth's crust: In theory, experiments, and geological application, Academic press, 1981.
- 50 Rowan, M. G.: Passive-margin salt basins: hyperextension, evaporite deposition, and salt tectonics, *Basin Research*, 26, 154–182, 2014.
- Rowan, M. G., Peel, F. J., and Vendeville, B. C.: Gravity-driven fold belts on passive margins, *AAPG Memoir*, 2004. 157–182, 2004.



- Rowan, M. G. and Vendeville, B. C.: Foldbelts with early salt withdrawal and diapirism: Physical model and examples from the northern Gulf of Mexico and the Flinders Ranges, Australia, *Marine and Petroleum Geology*, 23, 871–891, 2006.
- 5 Rudolf, M., Boutelier, D., Rosenau, M., Schreurs, G., and Oncken, O.: Rheological benchmark of silicone oils used for analog modeling of short-and long-term lithospheric deformation, *Tectonophysics*, 684, 12–22, 2016.
- Schellart, W.: Analogue modelling of large-scale tectonic processes: an introduction.(Ed.) Schellart, W. e Passchier, CW Analogue modelling of large-scale tectonic processes, *Journal of Virtual Explorer*, 7, 2002.
- 10 Stow, D. A. V., Huc, A. Y., and Bertrand, P.: Depositional processes of black shales in deep water, *Mar. Pet. Geol.*, 18, 491–498, 2001.
- Vendeville, B. C.: Salt tectonics driven by sediment progradation: Part I—Mechanics and kinematics, *AAPG Bull.*, 89, 1071–1079, 2005.
- Vendeville, B. C. and Jackson, M. P. A.: The fall of diapirs during thin-skinned extension, *Marine and Petroleum Geology*, 9, 354–371, 1992a.
- 15 Vendeville, B. C. and Jackson, M. P. A.: The rise of diapirs during thin-skinned extension, *Marine and Petroleum Geology*, 9, 331–354, 1992b.
- Warsitzka, M., Ge, Z., Schönebeck, J.-M., Pohlenz, A., and Kukowski, N.: Ring-shear test data of foam glass beads used for analogue experiments in the Helmholtz Laboratory for Tectonic Modelling (HelTec) at the GFZ German Research Centre for Geosciences in Potsdam and the Institute of Geosciences, Friedrich Schiller University Jena. GFZ Data Services, 2018.
- Warsitzka, M., Kley, J., and Kukowski, N.: Analogue experiments of salt flow and pillow growth due to basement faulting and differential loading, *Solid Earth*, 6, 9–31, 2015.
- Weinberger, R., Lyakhovsky, V., Baer, G., and Begin, Z. B.: Mechanical modeling and InSAR measurements of Mount Sedom uplift, Dead Sea basin: Implications for effective viscosity of rock salt, *Geochem. Geophys. Geosyst.*, 7, 2006.
- 25

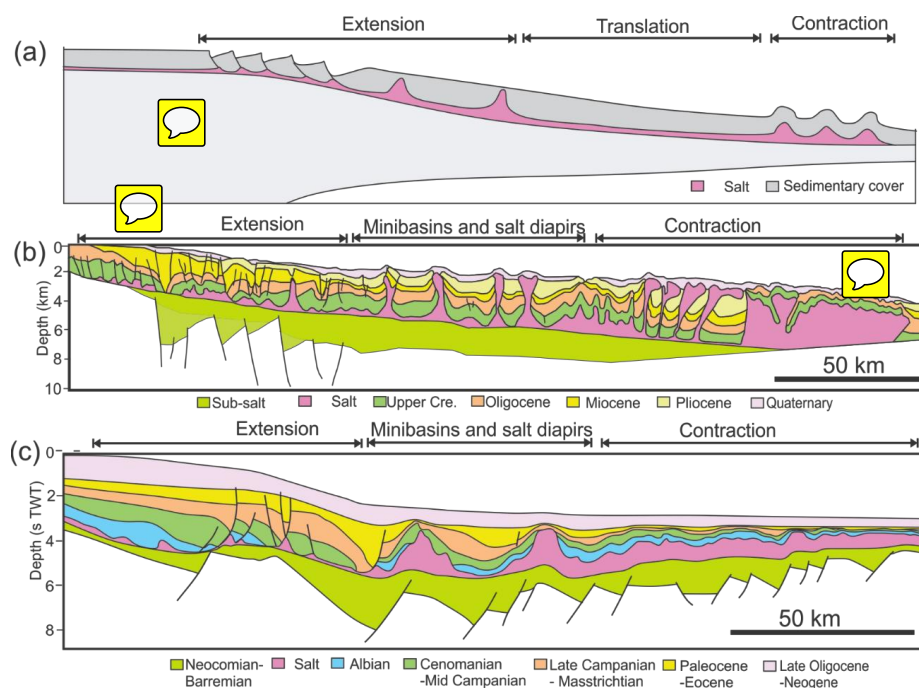


Figure 1. (a) Simplified cross section illustrating the kinematic domains and structural styles in a typical passive margin salt basin (modified after Rowan et al., 2004; Brun and Fort, 2011). (b) Regional interpreted seismic profile crossing the Lower Congo Basin (modified after Marton et al., 2000). Note the minibasins and diapirs in the mid-slope. (b) Regional interpreted seismic profile crossing the Central Santos Basin (modified after Modica and Brush, 2004). Note the large minibasin and diapirs in the mid-slope area.

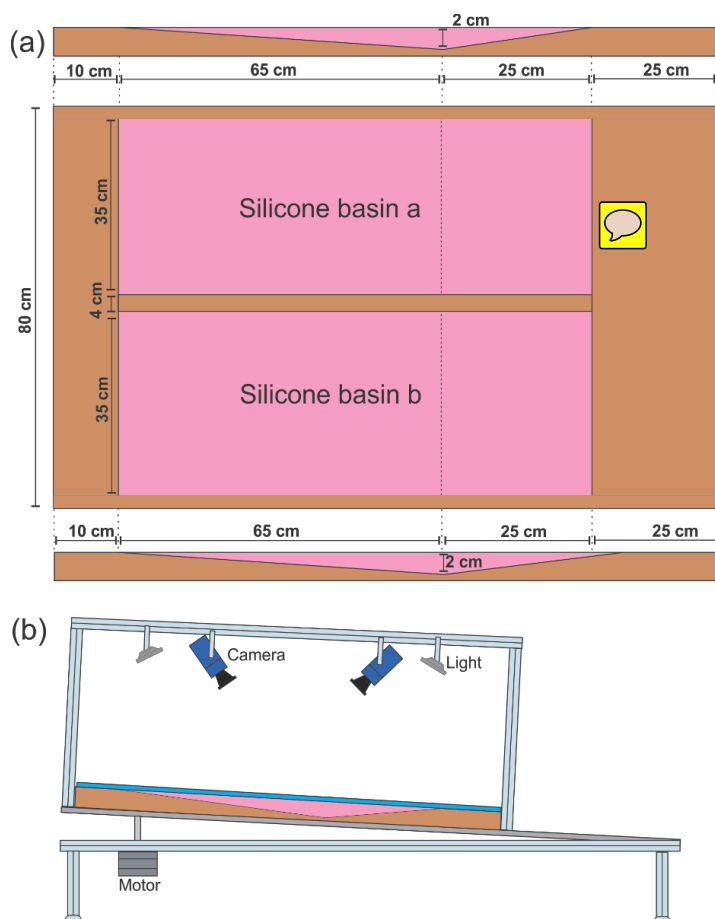


Figure. 2. Experimental setup and sketch of the apparatus. (a) Experimental setup of the two identical silicone basins. The double wedge shape of the silicone basin is 2 cm at its thickest. (a) 2D sketch of the experimental setup. The cameras are attached to the tilting basal plate pushed by the motor beneath.

5

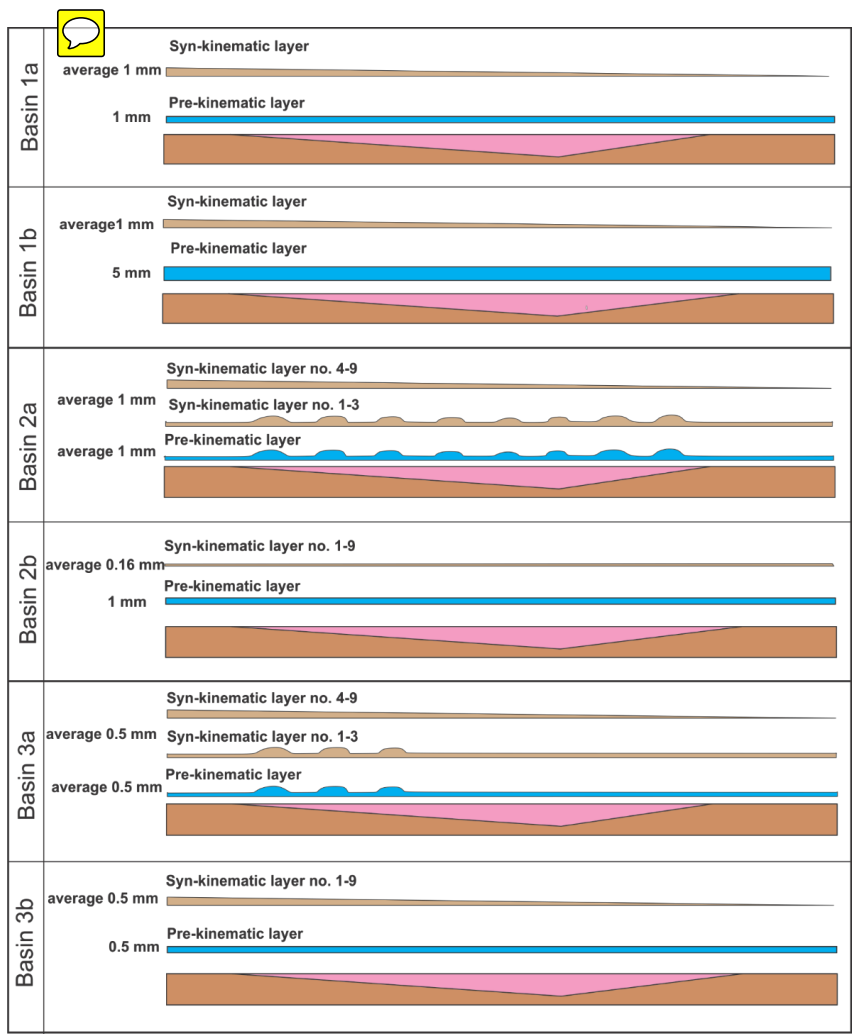


Figure. 3. Depositional scenarios for all six silicone basins of the three experiments. The blue layers are pre-kinematic layer and brown layers are syn-kinematic. Note the minibasin shape associates with differential loading in basins 2a and 3a. The syn-sedimentation thickness is in average as they are actually in wedge shape.

5

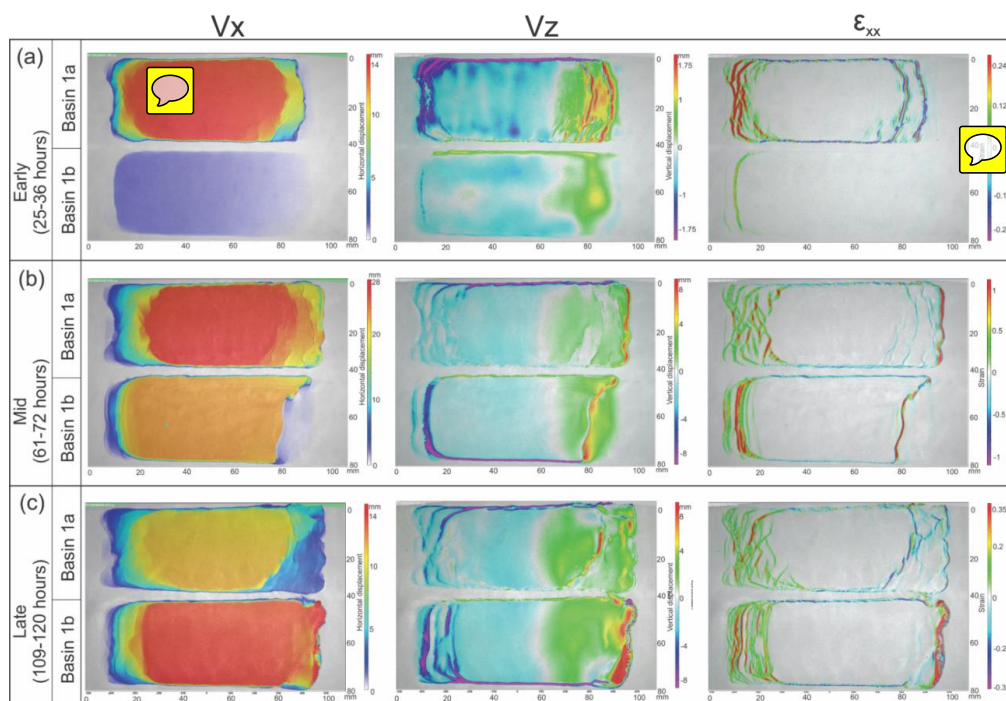


Figure 4. (a) Map view of finite horizontal displacement (V_x , V_z) and strain pattern (ϵ_{xx}) derived from 3D DIC strain data of experiment 1 from the (a) early (25–36 hours), (b) mid (61–72 hours) and (c) late stages (109–120 hours). The horizontal displacement (V_x) displays downslope displacement of the sedimentary cover (left to right in map view). The vertical displacement (V_z) displays total subsidence and uplift. Since the monitor system is attached to the apparatus, subsidence indicates net outflow of silicone and uplift indicates net inflow of silicone. The horizontal strain (ϵ_{xx}) shows location and strain magnitude of the extensional (red) and contractional (purple) structures. The large white space represents the translational domain between the extensional and contractional structures.

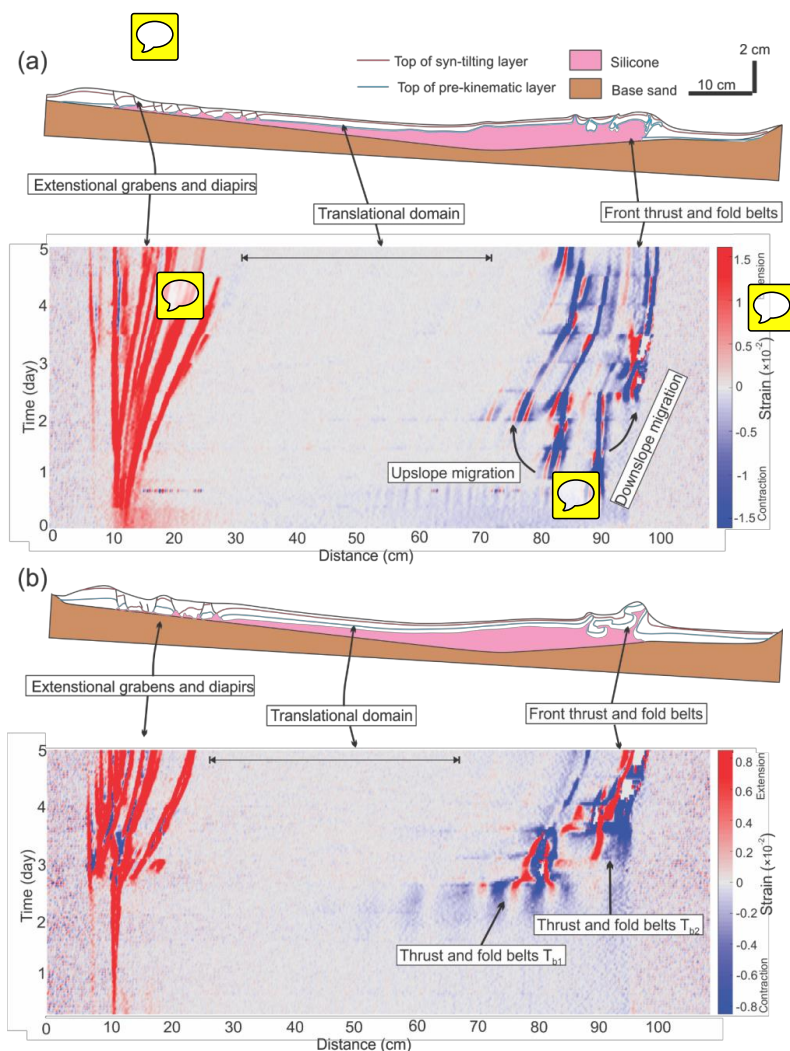


Figure 5. (a) Structural styles and kinematic domain partition in central section of Basin 1a. The strain plot of 1 hour interval along the central section beneath shows the initiation of extensional and contractional structures and how they evolved through time. Note the undeformed translational domain. (b) Structural styles and kinematic domain partition in central section of Basin 1b. The 1 hour strain plot through time shows the evolution of extensional and contractional structures in the central section. Note the contraction T_{b1} occurred in the mid stage during the experiment.

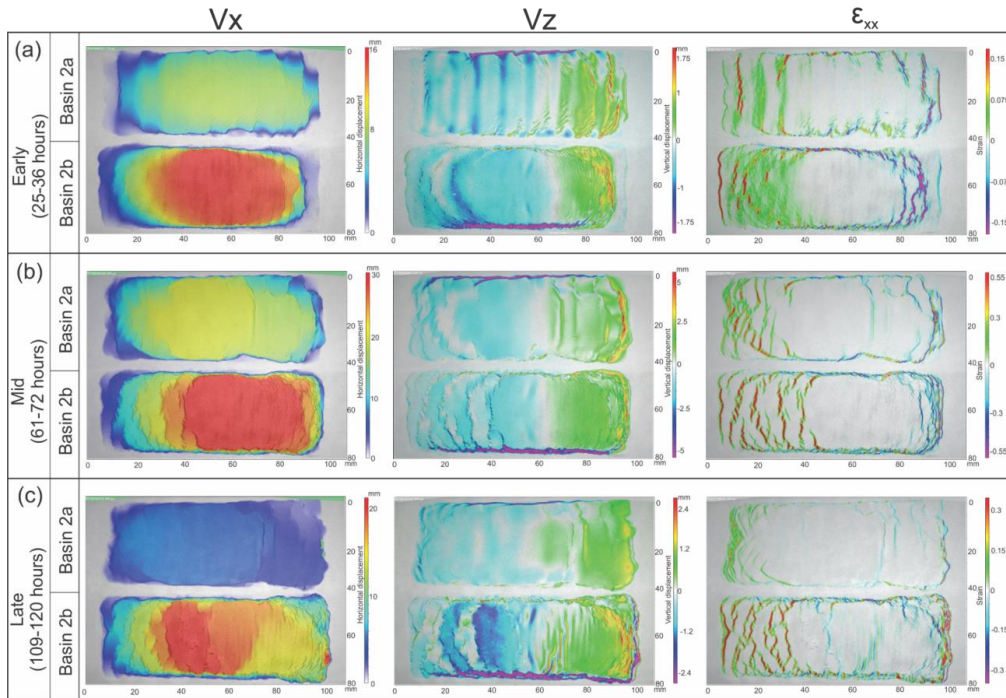


Figure 6. (a) Map view of finite horizontal displacement (V_x , V_z) and strain pattern (ϵ_{xx}) derived from 3D DIC strain data of the experiment 2 from the (a) early (25–36 hours), (b) mid (61–72 hours) and (c) late stages (109–120 hours). The horizontal displacement (V_x) displays downslope displacement of the sedimentary cover (left to right in map view). The vertical displacement (V_z) displays total subsidence and uplift. subsidence indicates net outflow of silicone and uplift indicates net inflow of silicone. Note the strings of subsidence of the Basin 2a in the early stage. The horizontal strain (ϵ_{xx}) shows the location and strain magnitude of the extensional (red) and contractional structures (purple). Note the basin-wide extension and contraction of the Basin 2b at late stage.

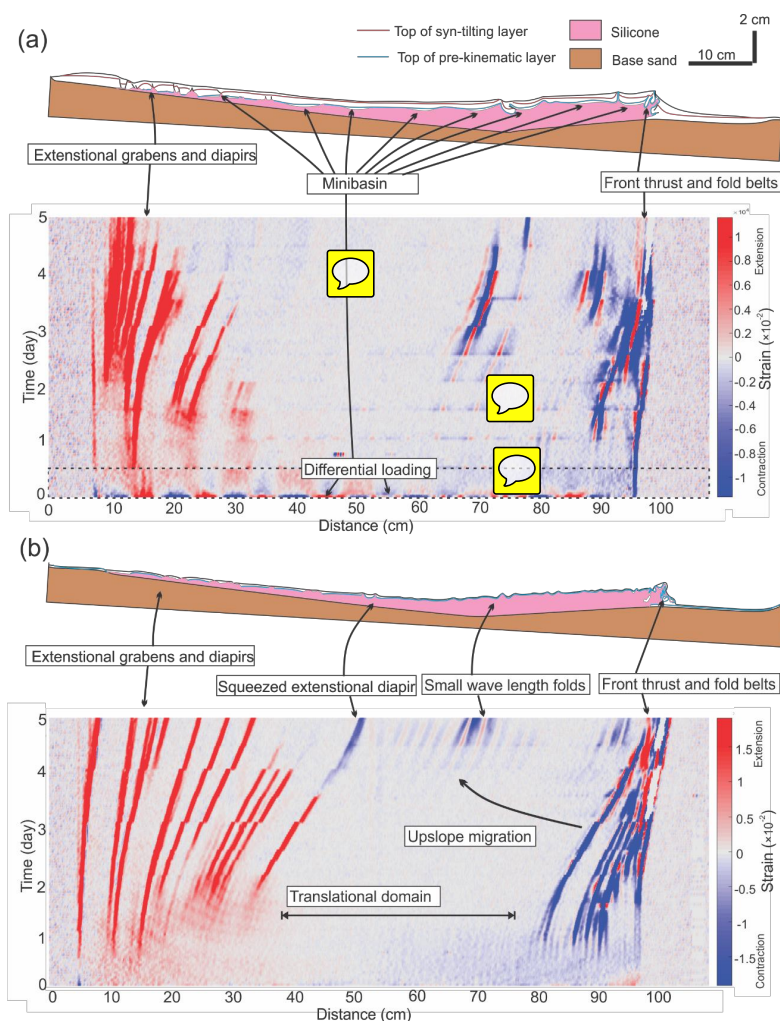


Figure 7. (a) Structural styles and kinematic domain partition in central location of the Basin 2a.

The strain plot of 1 hour interval along the central section beneath shows the initiation of extensional and contractional structures and how they evolved through time. Note the basin-wide extension and contraction in the first 6 hours of the experiment when differential loading was intentionally imposed onto the top of the silicone layer. The dash line box indicates the interval enlarged in Fig. 7c. (b) Structural styles and kinematic domain partition in central section of the Basin 2b. The strain plot (1 hour interval) through 5 days shows the evolution of extensional and contractional structures along central section. During the later stage the contractional domain migrated upward resulting in small wave length folding in the former translational domain. Some extensional diapirs get squeezed in the late stage.

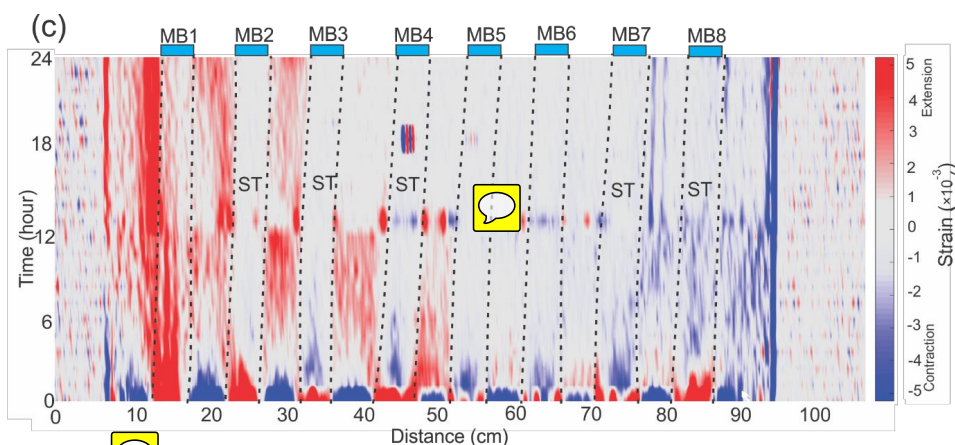


Figure 7 continue. (c) One hour interval strain profile of the first 24 hours along mid cross section of Basin 2a. The minibasins changed from areas of extension to zones that are relatively stable. MB means minibasin and ST means strain transfer. See Fig. 7a for the whole time interval of the first 24 hours.

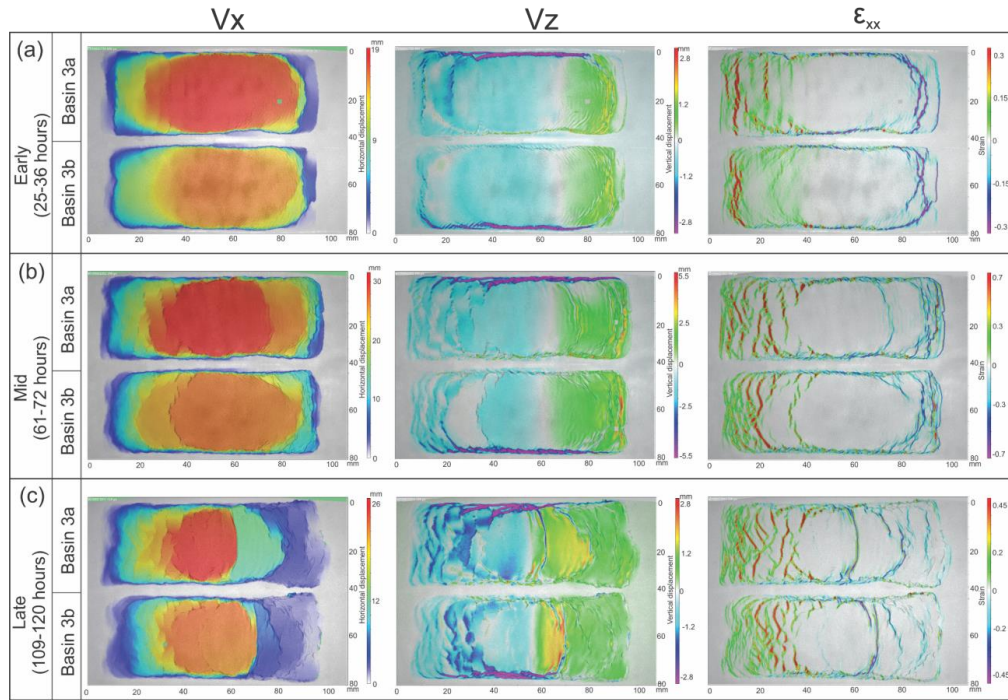


Figure 8. (a) Map view of finite horizontal displacement (V_x , V_z) and strain pattern (ϵ_{xx}) derived from 3D DIC strain data of the experiment 3 from the (a) early (25–36 hours), (b) mid (61–72 hours) and (c) late stages (109–120 hours). The horizontal displacement (V_x) displays downslope displacement of the sedimentary cover (left to right in map view). Note the decreasing of the red block from early to late in both basins indicating shrinking of the translational domain. The vertical displacement (V_z) displays total subsidence and uplift. The horizontal strain (ϵ_{xx}) shows the location and strain magnitude of the extensional (red) and contractional (purple) structures. Note the expansion of extension and contraction from early to late in both basins 3a and 3b.

10

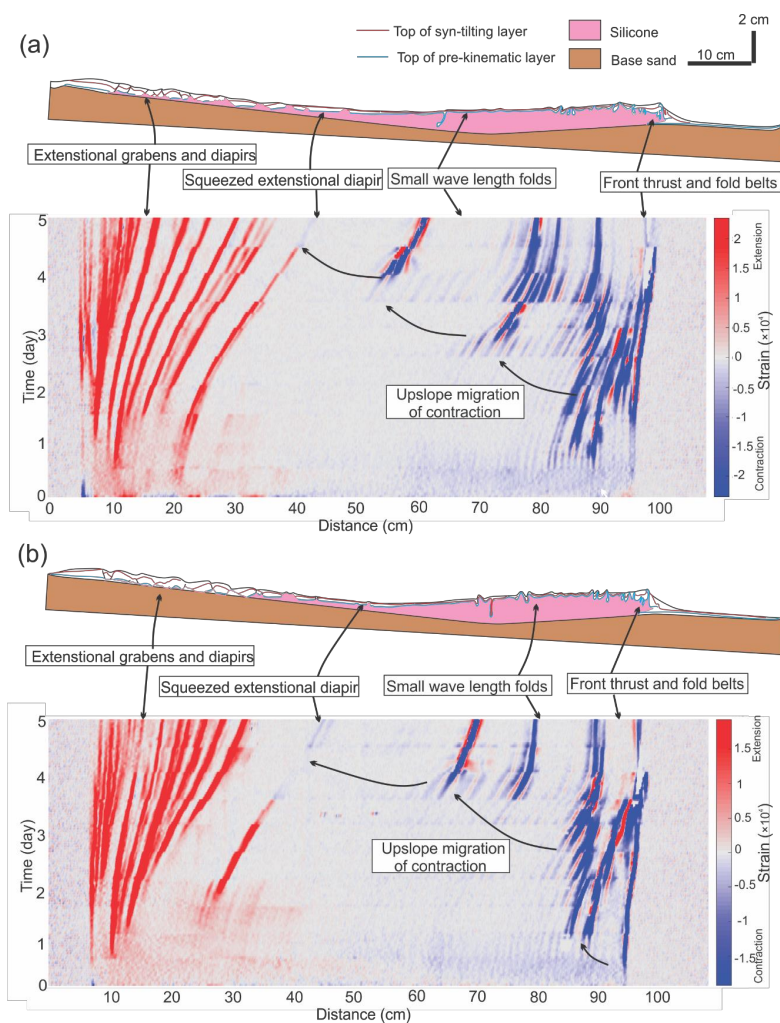


Figure 9 (a) Structural styles and kinematic domain partition in central section of Basin 3a. The strain plot of 1 hour interval along the central section shows the initiation of extensional and contractional structures and how they evolved through time. (b) Structural styles and kinematic domain partition in central section of Basin 3b. The strain plot of 1 hour interval through 5 days along the central section shows the evolution of extensional and contractional structures. Note the downslope migration of extensional domain and upslope migration of the contractional domain in both basins 3a and 3b.

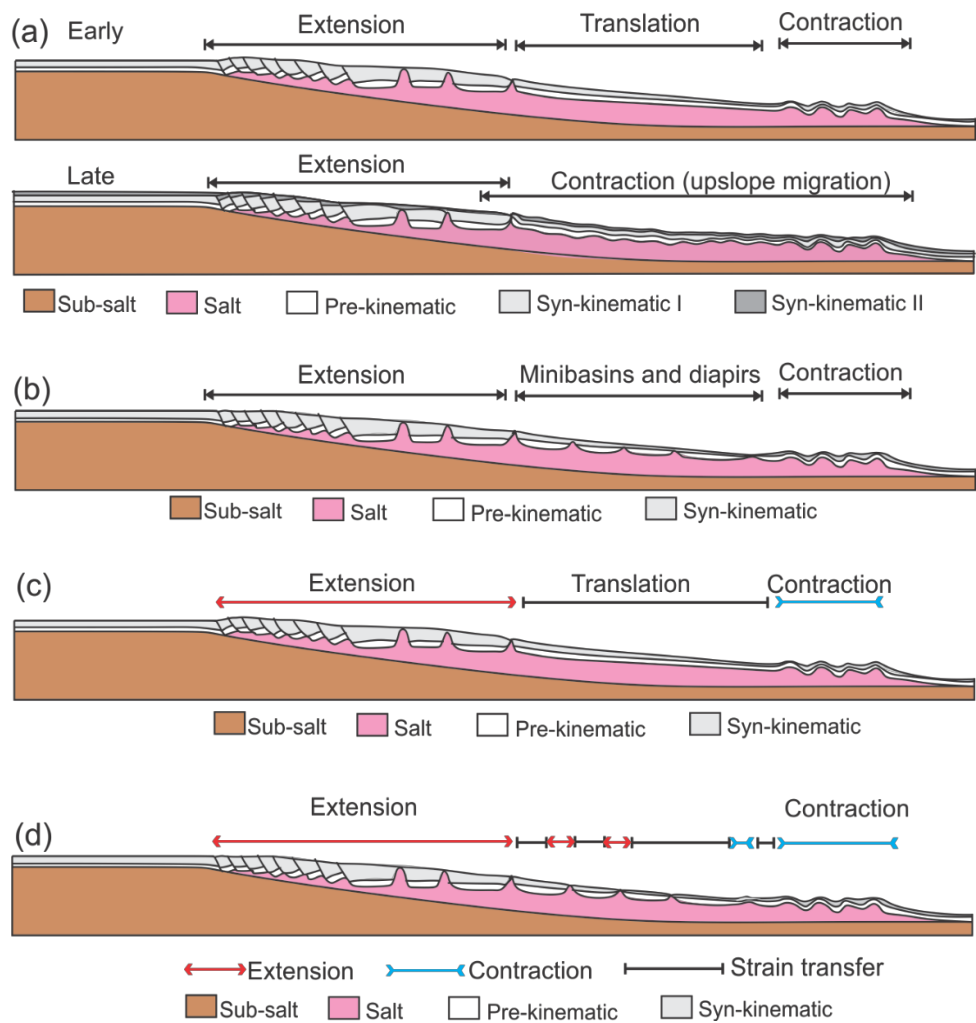


Figure 10. Mechanisms of deforming translational domain and models illustrating strain transfer with translational domain and minibasin with diapirs. (a) Low sedimentation rate and thin supra-salt cover allows upslope migration of contraction resulting in deformation of the translational domain. (b) Sedimentary differential loading lead to the development of minibasins and diapirs in the mid-slope preventing the establishment of a stable, undeformed translational domain. (c) The translational domain in the mid-slope allows strain transfer (ST) without internal deformation. (d) The minibasins and diapirs in the mid-slope allow strain transfer (ST) through a combination of movement of minibasin and stretching or squeezing of diapirs in between.



Appendix

| Quantity | Experiment (model) | Nature (prototype) | Scaling factor | Reference |
|----------------------|--|---|--|--|
| Length | $l_m = 1 \text{ cm}$ | $l_p = 1 \text{ km}$ | $l^* = [C/\rho g]_m / [C/\rho g]_p$ $l^* = 10^{-5}$ | Hubbert, 1937; Lallemand et al., 1994; Schellart, 2002 |
| Friction coefficient | $\mu_m = 0.55-0.75$ | $\mu_p = 0.4-0.8$ (1) | | (1) Ritter et al., 2016 |
| Cohesion | $C_m = 35-75 \text{ Pa}$ | $C_p = 5-20 \text{ MPa}$ (1) | | (1) Jaeger and Cook, 1969; Hoshino et al., 1972 |
| Density overburden | $\rho_m = 1130 \text{ kg m}^{-3}$ | $\rho_p = 2400 \text{ kg m}^{-3}$ | $\rho^* = 0.4708$ | |
| Gravity acceleration | $a_m = 9.8 \text{ m s}^{-2}$ | $a_p = 9.8 \text{ m s}^{-2}$ | $a^* = 1$ | |
| Stress | | | $\sigma^* = \rho^* a^* l^*$ $\sigma^* = 4.708 \times 10^{-6}$ | Hubbert, 1937; Ramberg, 1981 |
| Viscosity | $\eta_m = 2 \times 10^4 \text{ Pa s}$ PDMS silicone (1) | $\eta_p = 5 \times 10^{18} \text{ Pa s}$ from uplift rates (InSAR) of Dead Sea salt diapirs (2) | $\eta^* = 4 \times 10^{-15}$ | (1) Rudolf et al., 2016 (2) Weinberger et al., 2006 |
| Strain | | | $\epsilon^* = \sigma^* / \eta^*$ $\epsilon^* = 1.175 \times 10^9$ | Hubbert, 1937; Ramberg, 1981 |
| Time (subaerial) | Subaerial experiment $t_m = 1 \text{ h}$ | Subaerial salt basin $t_p = t_m / t^* = 0.134 \text{ Ma}$ | $t^* = 1/\epsilon^*$ $t^* = 8.51 \times 10^{-10}$ | Hubbert, 1937; Ramberg, 1981 |
| Time (submarine) | Subaerial experiment $t_m = 1 \text{ h}$ | Submarine salt basin $t_p = t_m / t_{sm}^* = 0.268 \text{ Ma}$ | $t_{sm}^* = 0.5 t^*$ $t_{sm}^* = 4.255 \times 10^{-10}$ | Gemmer et al., 2005 |

Table A1. Material properties and Scaling of the experiments in this study. Note geometric scaling of 1cm in model is 1 km in nature and time scaling of 1 hour in model is 0.268 Ma in nature.



| My (P) | Time in Hr (M) | Sedimentation thickness | Basin 1b | Basin 1b | Basin 2a | Basin 2b | Basin 3a | Basin 3b |
|--------|----------------|-------------------------|----------|----------|--------------|----------|----------------|----------|
| 0 | 0 | Pre-kinematic | 1 mm | 5 mm | 1 mm with DF | 1 mm | 0.5 mm | 0.5 mm |
| 1 | 4 | | | | | | | |
| 2 | 8 | | | | | | | |
| 3 | 12 | Syn-sedimentation 1 | 1 mm | 1 mm | 1 mm with DF | 0 | 0.5 mm with DF | 0.5 mm |
| 4 | 16 | | | | | | | |
| 5 | 20 | | | | | | | |
| 6 | 24 | Syn-sedimentation 2 | 1 mm | 1 mm | 1 mm with DF | 0 | 0.5 mm with DF | 0.5 mm |
| 7 | 28 | | | | | | | |
| 8 | 32 | | | | | | | |
| 9 | 36 | Syn-sedimentation 3 | 1 mm | 1 mm | 1 mm with DF | 0.14 mm | 0.5 mm with DF | 0.5 mm |
| 10 | 40 | | | | | | | |
| 11 | 44 | | | | | | | |
| 12 | 48 | Syn-sedimentation 4 | 1 mm | 1 mm | 1 mm | 0.17 mm | 0.5 mm | 0.5 mm |
| 13 | 52 | | | | | | | |
| 14 | 56 | | | | | | | |
| 15 | 60 | Syn-sedimentation 5 | 1 mm | 1 mm | 1 mm | 0.12 mm | 0.5 mm | 0.5 mm |
| 16 | 64 | | | | | | | |
| 17 | 68 | | | | | | | |
| 18 | 72 | Syn-sedimentation 6 | 1 mm | 1 mm | 1 mm | 0.2 mm | 0.5 mm | 0.5 mm |
| 19 | 76 | | | | | | | |
| 20 | 80 | | | | | | | |
| 21 | 84 | Syn-sedimentation 7 | 1 mm | 1 mm | 1 mm | 0.12 mm | 0.5 mm | 0.5 mm |
| 22 | 88 | | | | | | | |
| 23 | 92 | | | | | | | |
| 24 | 96 | Syn-sedimentation 8 | 1 mm | 1 mm | 1 mm | 0.31 mm | 0.5 mm | 0.5 mm |
| 25 | 100 | | | | | | | |
| 26 | 104 | | | | | | | |
| 27 | 108 | Syn-sedimentation 9 | 1 mm | 1 mm | 1 mm | 0.27 mm | 0.5 mm | 0.5 mm |
| 28 | 112 | | | | | | | |
| 29 | 116 | | | | | | | |
| 30 | 120 | Stop | Stop | Stop | Stop | Stop | Stop | Stop |



Table A2. Sedimentation rates, pre- and syn-kinematic depositional scenarios for all six silicone basins of the three experiments m – model, p - prototype.

